Superradiant parametric conversion of spin waves

Mateusz Mazelanik,[1,2,*] Adam Leszczyński,[1,2] Michał Lipka,[1,2] Wojciech Wasilewski,[1] and Michał Parniak[1,3,†]

[1]*Centre for Quantum Optical Technologies, Centre of New Technologies, University of Warsaw, Banacha 2c, 02-097 Warsaw, Poland*

[2]*Faculty of Physics, University of Warsaw, Pasteura 5, 02-093 Warsaw, Poland*

[3]*Niels Bohr Institute, University of Copenhagen, Blegdamsvej 17, DK-2100 Copenhagen, Denmark*

(Received 21 July 2019; revised manuscript received 26 October 2019; published 22 November 2019)

Atomic-ensemble spin waves carrying single-photon Fock states exhibit nonclassical many-body correlations in between atoms. The same correlations are inherently associated with single-photon superradiance, forming the basis of a plethora of quantum light-matter interfaces. We devise a scheme allowing the preparation of spatially structured superradiant states in the atomic two-photon cascade using spin-wave light storage. We thus show that long-lived atomic ground-state spin waves can be converted to photon pairs, opening the way towards nonlinear optics of spin waves via multi-wave-mixing processes.

DOI: 10.1103/PhysRevA.100.053850

I. INTRODUCTION

Spatially extended atomic ensembles are a particularly versatile medium, allowing generation and control of light with widely varying properties. Fulfillment of the phase-matching (PM) condition facilitates efficient generation, storage, and retrieval of single photons. Superradiance is inherently linked to the phase-matched emission and, in particular, spin waves (SW) that store information about light in the atomic coherence are superradiant Dicke states $N^{-1/2}\sum_j e^{i\mathbf{Kr}_j}|g_1 \ldots h_j \ldots g_N\rangle$ [1]. In practice, the Λ scheme of atomic levels, which forms the basis of the Duan-Lukin-Cirac-Zoller (DLCZ) quantum entanglement distribution protocol [2], is well known for its capabilities to generate photon pairs [3,4] with both nontrivial temporal [5] and spatially multimode structure [6,7]. There, light is interfaced with a coherence between two metastable ground-state sublevels.

An alternative ladder or diamond schemes allow generation of two-color photon pairs and attract much attention [8–11] also for single-photon storage [12,13] and in Rydberg-blockaded media [14,15]. In those cases the associated SWs lie between a ground state and an excited atomic state and are intermediate steps in the generation of a photon pair. More complex manipulations of those SWs, such as temporal [16–20] and spatial [21] multi-SW beamsplitters demonstrated for ground-state SWs, remain elusive. Such control would allow SW-based engineering of photon pair emission, possibly also extensible to deterministic quantum nonlinear optics based on Rydberg atoms [22].

The atomic-ensemble-based schemes hold some advantages over spontaneous parametric downconversion processes (SPDC) in nonlinear crystals and optical parametric oscillators [23–25], which also rely on engineered PM, as the photons generated in atomic ensembles are inherently narrow band and atom resonant, making them suitable for quantum metrology [26] and repeater-based communication [2,27,28]. With a purely atomic photon-pair source, potentially difficult engineering of cavity-based SPDC can be avoided [29,30].

Here we show that the properties of a phase-matched cascaded atomic decay can be engineered via proper preparation of the atomic SW state. In particular, we treat the SW prepared in the Raman process as one of the fields participating in the parametric conversion, similarly as a pump field in SPDC in nonlinear crystals [23]. Hitherto schemes necessarily required that the atom starts and ends the wave-mixing processes in the same ground state, as dictated by the principles of energy and momentum conservation. This requirement can be leveraged if the ensemble is first prepared in a superposition state, or in other words, some coherence is present. Our scheme allows for complex engineering of two-photon emission, with atom-resonant photons without the need of cavities.

We generate a strong atomic coherence (SW) between $|g\rangle$ and $|h\rangle$ via Raman interaction in the Λ scheme, as depicted in Fig. 1(a). The two pump fields (P1 and P2), as in Fig. 1(b), then transfer the coherence $|g\rangle\langle h|$ via a two-photon process to the $|g\rangle\langle c|$ involving the highest excited state. The standard coherent two-photon decay follows, by the end of which the atom returns to its ground state $|g\rangle$. The entire process can be viewed as a two-step spontaneous six-wave mixing (6WM) with a time delay, previously demonstrated for classical beams [31], which conserves both momentum and energy overall.

This unorthodox view leads to numerous implications, as the SW may be manipulated in various ways, including usage of magnetic [32–34], electric [35], and optical fields [16,21,36–38]. Reshaping the SW structure will subsequently result in a modified atomic state during emission of the idler photon. Such a modification can serve to change the properties of superradiance, facilitating better understanding of this collective process and harnessing it in bulk atomic ensembles. From the quantum information perspective, both polarization as well as temporal and spatial properties of the generated biphoton wave function can be modified, leading to complex multi-degree-of-freedom entangled states.

*m.mazelanik@cent.uw.edu.pl

†m.parniak@cent.uw.edu.pl

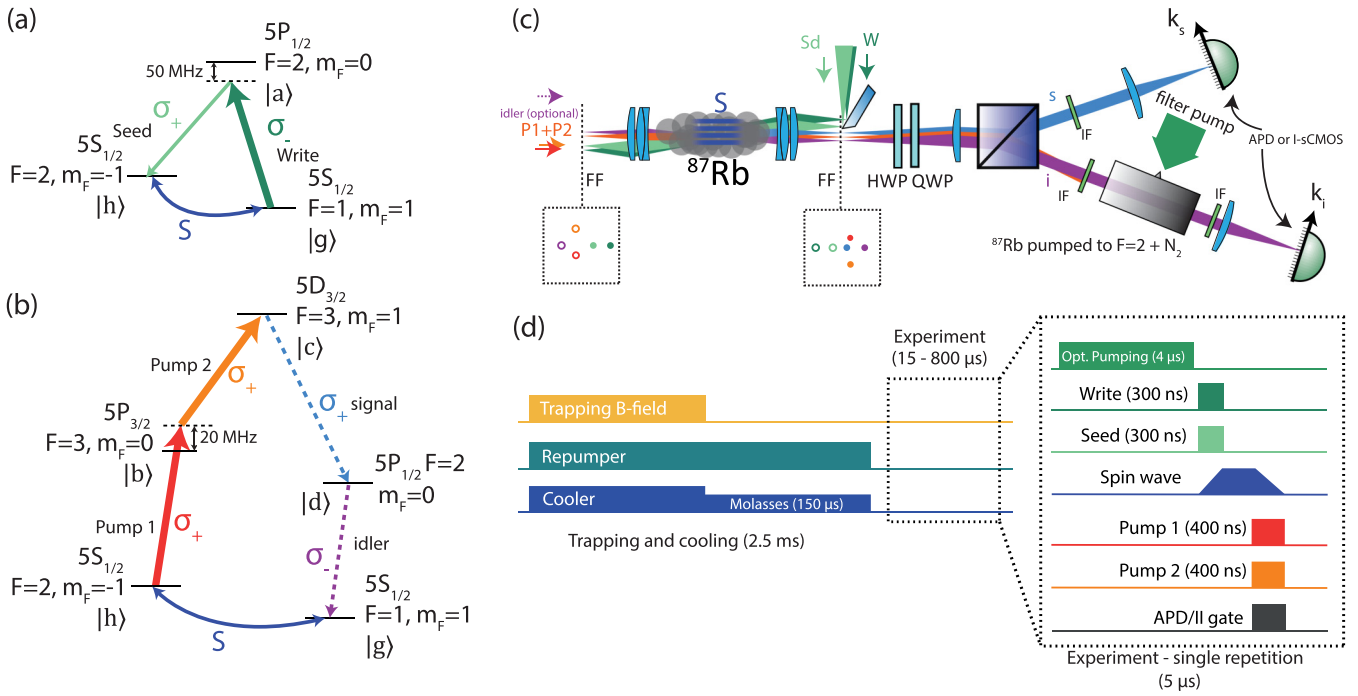

FIG. 1. Experimental setup details. (a) Rubidium-87 levels configuration used to generate ground-state SW via seeded Raman scattering in the first step of the delayed 6WM scheme. (b) Relevant energy levels used to generate correlated photon pairs via spontaneously induced two-photon decay closing the 6WM scheme. (c) Schematic of the experimental setup used to observe correlated photon pairs generated within the delayed 6WM scheme (P1 - pump1, P2 - pump 2, W - write, Sd - seed, FF - far field, IF - interference filter). (d) Time sequence of the experiment detailing the order of all experimental steps leading to correlated photon pair generation.

The ladder- [39–41] and diamond-type [42–44] systems have previously been successfully used to generate photons with particularly good characteristics. The key advantages of these schemes applied to rubidium are the possibility to generate one of the photons at telecom wavelength [45–47] and relaxed requirements for filtering, even in room-temperature ensembles [11,48,49], as compared with the Λ scheme. Previous preliminary studies have suggested that excited–to–excited-state transition could be used for readout of a ground-state atomic coherence [31,50].

A striking feature of the two-photon decay is the superradiant enhancement of emission [1,10,39], observed both in ultracold and warm atomic ensembles at high optical depths. Superradiance, while previously observed in many systems, here is shown to be controlled within the spatial domain. Our system thus contributes to recent fundamental studies of superradiant emission in cold atoms [51–53]. Among many intricacies, this behavior proves the role of atomic coherence in the process.

II. EXPERIMENT

We start the experiment by employing two coherent optical fields (write and seed, both 795 nm) to generate macroscopic ground-state atomic coherence ρ_{hg} between states $|g\rangle$ and $|h\rangle$ in a cold ^{87}Rb atomic ensemble [see Fig. 1(a) and Appendix A for details]. This coherence, commonly called a spin wave, has a nontrivial spatial dependence $\rho_{hg}(\mathbf{r}) \propto \exp(i\mathbf{K}\mathbf{r})$, where $\mathbf{K} = \mathbf{k}_W - \mathbf{k}_{Sd}$ is a SW wave vector and $\mathbf{k}_W$, $\mathbf{k}_{Sd}$ are wave vectors of the write and seed fields, respectively.

In next step we use a pair of strong laser fields (pumps 1 and 2) to transform a substantial part of excitations of state $|h\rangle$ into state $|c\rangle$, creating an excited state SW: $\rho_{cg}(\mathbf{r}) \propto \rho_{hg} \exp[i(\mathbf{k}_{P1} + \mathbf{k}_{P2})\mathbf{r}]$, where $\mathbf{k}_{P1}$, $\mathbf{k}_{P2}$ are the wave vectors of the pumps 1 and 2, respectively. For clarity, assuming large diameters of pumps 1 and 2 beams, we define the excited state SW as

$$\mathcal{S}(\mathbf{r}) \equiv \sqrt{n(\mathbf{r})}\rho_{cg}(\mathbf{r}) = \sqrt{n(\mathbf{r})}\beta e^{i(\mathbf{K}+\mathbf{k}_{P1}+\mathbf{k}_{P2})\mathbf{r}}, \qquad (1)$$

where the complex SW amplitude β incorporates all the phase shifts between pump fields, and by $n(\mathbf{r})$ we denote the local atom density. The presence of $\mathcal{S}$ enables a spontaneously induced coherent two-photon transition to the original ground-state level $|g\rangle$, closing the 6WM scheme.

The transition happens in two steps: first the spontaneously emitted signal photon transfers one collective excitation of $|c\rangle$ to the intermediate state $|d\rangle$, conditionally creating a Fock-state SW between levels $|d\rangle$ and $|g\rangle$ from which the superradiantly enhanced emission of the idler photon occurs. Thus, the idler photon is emitted always after the signal photon.

The whole quantum amplitude $\psi(t_s, t_i, \mathbf{k}_{s\perp}, \mathbf{k}_{i\perp})$ of the generated biphoton state exhibits two features: the spatial and temporal correlation. Here, however, we study these features separately and thus we will define two proper objects: the time-averaged spatial wave function $\psi_k(\mathbf{k}_{s\perp}, \mathbf{k}_{i\perp}) = \langle\psi(t_s, t_i, \mathbf{k}_{s\perp}, \mathbf{k}_{i\perp})\rangle_t$ and the temporal wave function $\psi_t(t_s, t_i)$ for a fixed pair of $\{\mathbf{k}_{s\perp}, \mathbf{k}_{i\perp}\}$.

From quantum perturbation theory (see Appendix B for the derivation using Hamiltonian treatment) for weak signal and idler fields, assuming that the atom density $n(\mathbf{r})$ is described

by the Gaussian distribution with longitudinal width equal to σ_z, we can write the spatial part as

$$\psi_k(\mathbf{k}_{s\perp}, \mathbf{k}_{i\perp}) \propto \tilde{n}(\Delta\mathbf{k}_\perp) e^{-\Delta k_z^2 \sigma_z^2}, \tag{2}$$

where by $\tilde{n}$ we denote the Fourier transform of the atomic density, and the transverse wave-vector mismatch is defined as follows: $\Delta\mathbf{k}_\perp = \mathbf{K}_\perp + \mathbf{k}_{P1\perp} + \mathbf{k}_{P2\perp} - \mathbf{k}_{s\perp} - \mathbf{k}_{i\perp}$. By

$$\Delta k_z \equiv K_z + \sqrt{k_{P1}^2 - k_{P1\perp}^2} + \sqrt{k_{P2}^2 - k_{P2\perp}^2} - \sqrt{k_s^2 - k_{s\perp}^2} - \sqrt{k_i^2 - k_{i\perp}^2} \tag{3}$$

we denote the longitudinal wave-vector mismatch.

The temporal part can be approximated with the following form [54]:

$$\psi_t(\tau) = \mathcal{N} e^{-\tau/2\tau_0} \Theta(\tau), \quad \tau = t_s - t_i. \tag{4}$$

Importantly, the time constant τ_0 depends on the particular geometrical configuration, i.e., the PM, exposing the nontrivial connection of the temporal and spatial properties of the generated state.

The experimental setup details are provided in Fig. 1(c). The signal, idler, and all of the control beams (including pumps as well as write and seed) are combined in the far field (FF) of the ensemble and propagate along the z axis. Since the signal and idler fields closing the 6WM process have orthogonal polarizations (respectively $\sigma^+$and σ^-), we separate them using a quarter-wave plate and Wollaston prism. Then, after passing the interference filters (IF), depending on the situation they are either detected on the Intensified-sCMOS camera [55] situated in the far field of the ensemble or coupled to single-mode fibers connected to single-photon counting modules (SPCMs). To filter out uncorrelated 795-nm photons coming from the $5P_{1/2}, F = 2 \rightarrow 5S_{1/2}, F = 2$ decay path, we employ an additional filtering consisting of a glass cell containing optically pumped to $5S_{1/2}, F = 2$ state rubidium-87 vapor and buffer gas (nitrogen, 10 Torr). For alignment purposes we send an additional beam indicated as an incoming idler in Fig. 1(c) to seed the signal-idler (SI) generation process and observe the classically generated signal beam. For the temporal correlations measurements we first observe the generated signal beam and maximize its amplitude in the sense of satisfying the PM condition $\Delta k_z = 0$. Then we couple this signal beam to the single-mode mode fiber of the signal SPCM. The particular experimental configuration, i.e., control beam angles and propagation direction, was chosen to provide a broad PM spatial spectrum, while the particular choice of atomic states and polarizations was motivated by minimization of loss and noise. Essentially, by selecting the $F = 3$ manifold as the first intermediate state $|b\rangle$ we avoid performing a read-out of the SW with the pump 1 field. Still, the pump 1 field rescatters excitation to other magnetic states of the $F = 2$ ground-state manifold, causing effective decoherence of the SW. In Fig. 1(d) we present the time sequence of the experiment, including all the steps described above.

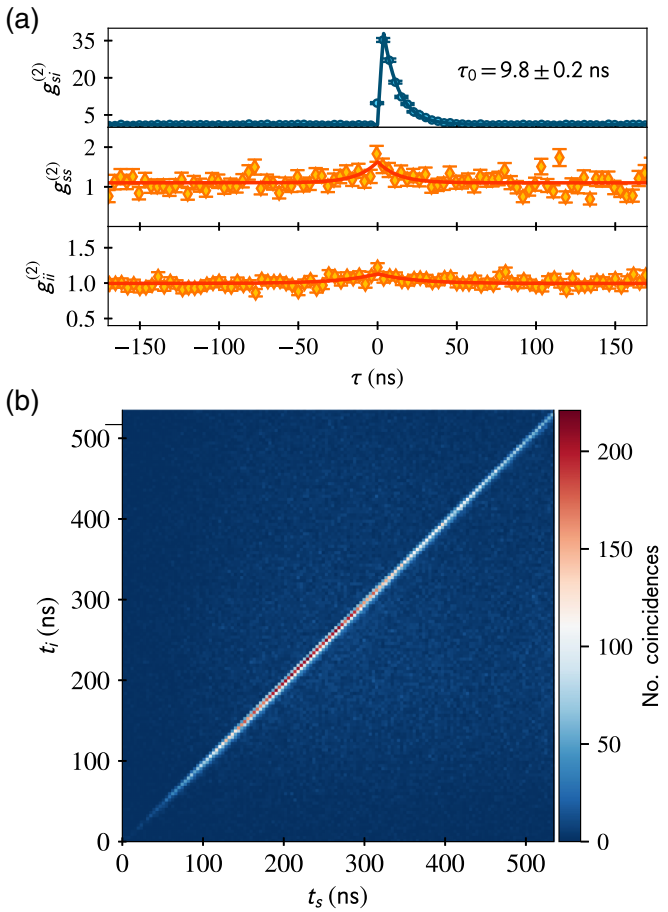

FIG. 2. (a) Measured second-order correlation functions between signal and idler fields $g_{si}^{(2)}(\tau = t_i - t_s)$ for the two possible decay paths through different intermediate levels $|d\rangle$ ($m_F = 0$) and autocorrelation functions $g_{jj}^{(2)}(\tau = t_{j1} - t_{j2})$ for the signal ($j = s$) and idler ($j = i$) fields. Registered photon rate amounts to 6×10^{-3} photon/μs for signal photons. (b) Raw signal-idler coincidence data for the cross-correlation accumulated during the entire pulse.

III. TEMPORAL CORRELATIONS

We first present the measurement of temporal correlations in a particular, preselected wave-vector configuration. Figure 2(a) depicts a histogram of SI correlation as a function of mutual delay, where we fit the second-order cross-correlation as $g_{si}^{(2)}(\tau) = 1 + \alpha |\psi_t(\tau)|^2 * h(\tau)$. By introducing convolution with $h(\tau) = [\Theta(\tau) - \Theta(\tau - \delta t)]/\delta t$ we account for a finite time resolution $\delta t = 3.85$ ns of the time tagging module. We observe a very strong correlation $g_{si}^{(2)}(0) = 35.3 \pm 0.8$, with simultaneously measured autocorrelations $g_{ii}^{(2)}(0) = 1.11 \pm 0.06$ and $g_{ss}^{(2)}(0) = 1.13 \pm 0.16$. These two measurements constitute a strong violation of the Cauchy-Schwarz inequality [56] with

$$R = \left(g_{si}^{(2)}\right)^2 / \left(g_{ss}^{(2)} g_{ii}^{(2)}\right) = 986 \pm 153 \gg 1. \tag{5}$$

We measure coincidences during the P1+P2 pulse transferring the ground-state SW to the exited state $|c\rangle$, which last approximately 300 ns, as well as during a subsequent decay. We observed that if the excitation pulse is applied continuously, decoherence of the SW ρ_{hg} by pump P1 is

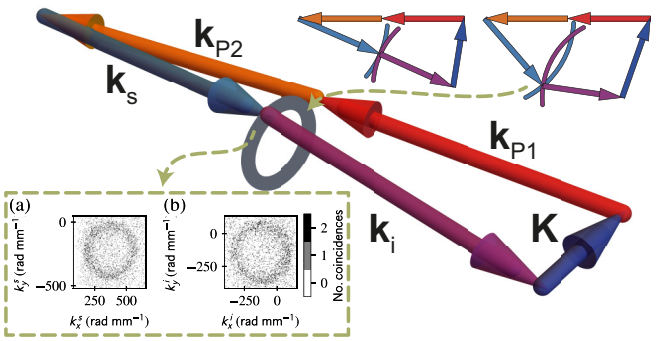

FIG. 3. Three-dimensional configuration of the wave vectors of all fields interacting in the second part of the delayed 6WM scheme. The shape encircled by the $\mathbf{k}_s$ wave-vector indicates the set of SI emission directions $\{\mathbf{k}_s, \mathbf{k}_i\}$ satisfying the PM condition $\Delta k_z = 0$. In the insets we plot measured signal (a) [idler (b)] photon count distribution conditioned on correlated ($|\Delta\mathbf{k}_\perp| \leqslant \delta k$) idler (signal) photon events.

strong and the number of coincidences decreases. Quite similarly, even during the decay of the $|c\rangle$ state we observed that the initial period yields the highest signal-to-noise ratio effectively represented by $g^{(2)}_{si}$. We attribute this effect to a thermal decay [57] of $\mathcal{S}$. In Fig. 2(b) we present additional data showing the temporal evolution of signal-idler correlation during the two-photon coherence transfer (creation of $\mathcal{S}$) and the subsequent decay. Indeed, even with negligible K (length of ground-state SW wave vector), the longitudinal component of $\mathcal{S}$ is $K_{\mathcal{S},z} = 2\pi(\frac{1}{\lambda_{P1}} + \frac{1}{\lambda_{P2}}) \approx 1.6 \times 10^4$ rad/mm, yielding a motional characteristic Gaussian decay time of $\tau_T^{-1} = |\mathbf{K}_\mathcal{S}|\sqrt{k_B T/m_{\mathrm{Rb}}} \approx 0.7/\mu$s.

We measure the correlation time $\tau_0 = 9.8 \pm 0.2$ ns, which suggests a strong role of superradiance in the process, as without superradiant emission enhancement we would expect $\tau_0 = 27.7$ ns, which is a natural lifetime of state $|d\rangle$. Furthermore, thermal decoherence of SW $|h\rangle\langle d|$ and any magnetic decoherence are much slower. With this we experimentally prove that superradiance is inherently linked to PM emission [58] and can occur in any wave-mixing process. Here, it is demonstrated in 6WM.

IV. WAVE-VECTOR DOMAIN CORRELATIONS

In the second experiment we analyze SI correlations in the wave-vector space. Using the I-sCMOS camera we collected 5M frames for each of five different values of the SW wave vector $\mathbf{K}$. Here, the $g^{(2)}_{si}(\mathbf{k}_\perp = \mathbf{k}_{P1\perp} + \mathbf{k}_{P2\perp} - \mathbf{k}_{s\perp} - \mathbf{k}_{i\perp})$ is calculated in the wave-vector-sum coordinates with shifted variables by the sum of transverse components of pump wave vectors (see Fig. 3 for the full wave-vector configuration). In this configuration, we expect that the correlation peak will appear in the spot $\mathbf{k}_\perp = \mathbf{K}_\perp$ determined by the initial SW. This is indeed what we observed in Figs. 4(a)–4(e). Note that the correlations are averaged over the entire duration of the pulse, which we denote by $\langle g^{(2)}_{si}\rangle_\tau$. The averaging, with the pair-generation rate yielding 0.5 signal photons detected per frame on average, leads to significantly lower values for the cross-correlation than in Fig. 2(a). The PM condition renders the SI emission cones and thus, we expect that correlated signal and idler pairs will appear in ring-shaped regions on the camera. To verify that we filter SI events by choosing only those for which $|\Delta\mathbf{k}_\perp| \leqslant \delta k$, where by introducing $\delta k = 15$ rad mm^{-1} we account for a finite spread of the correlation peak. In

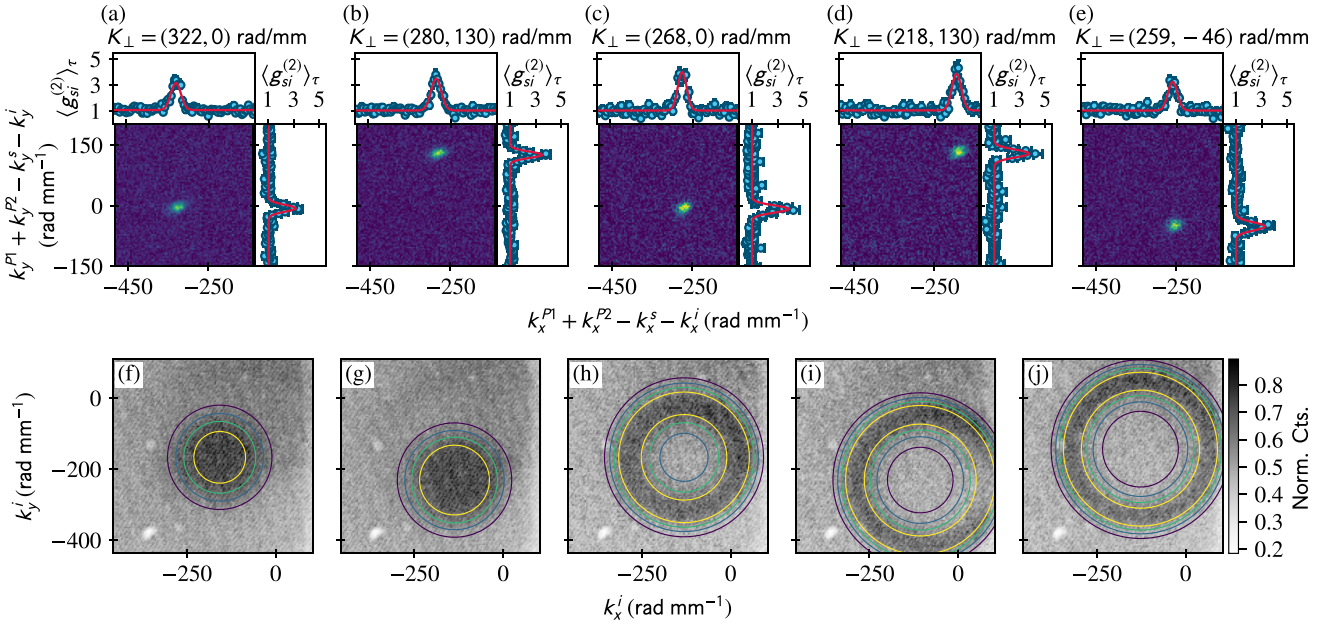

FIG. 4. Correlation functions and superradiant emission patterns measured for a set of the ground-state SW wave vectors. (a)–(e) Sum of momenta coordinates SI second-order correlation function $\langle g^{(2)}_{si}\rangle_\tau$ maps for different ground-state SWs. The correlation peak emerges from PM condition $\Delta k_z = 0$, and its position indicates the SW transverse components $\mathbf{K}_\perp = (K_x, K_y)$. (f)–(j) Accumulated idler photon counts for approximately 5M experiment repetitions. The contour plots are the theoretical predictions of the PM. The data correspond to the same experimental situation columnwise.

insets (a, b) of Fig. 3 we plot signal and idler accumulated events after the filtering procedure. We see that the correlated photons mostly come from the ring-shaped regions.

Finally, we show that the PM patterns are most easily recovered by looking at the absolute intensity of the registered idler light channel to phase-matched regions by superradiance. The intensity in perfectly correlated regions is increased approximately twofold [see Figs. 4(f)–4(j)]. This can be understood as an interplay between coherent and incoherent emission. The signal photon is emitted in a random direction, leading to a creation of a random SW ρ_{dg}. In most cases this SW either does not lead to phase-matched emission (see Fig. 3) or decoheres rapidly due to atomic motion. A photon associated with such excitation is thus emitted in a random direction, in particular also in the PM cone. This cone is quite narrow, and there the PM leads to expected coherent emission of the idler photon. Thus, starting with a mean SW number $\bar{n}$ per pixel, we arrive at still roughly $\eta\bar{n}$ incoherent idler photons per pixel and additional $\bar{n}_{\mathrm{coh}} = \eta\bar{n}$ coherent emission into the phase-matched region. This number, and thus the ratio $(\bar{n} + \bar{n}_{\mathrm{coh}})/\bar{n}$, may be decreased due to incoherent excitation of the SW field ρ_{hg}, incoherent transfer to $\mathcal{S}$, as well as its motional decoherence. The actual value which we obtain in the experiment is $(\bar{n} + \bar{n}_{\mathrm{coh}})/\bar{n} \approx 1.4$.

We compare the expected shape of phase-matched regions described by

$$\bar{n}_{\mathrm{coh}}(\mathbf{k}_{i\perp}) \propto \int e^{-2\Delta K_z(\mathbf{k}_{s\perp},\mathbf{k}_{i\perp})^2\sigma_z^2} d^2\mathbf{k}_{s\perp}, \tag{6}$$

with the observed shapes of regions of increased idler count rates. Without fitting (since all parameters are determined from correlation measurement), we observe very good agreement of the shape between experiment and theoretical prediction.

In Fig. 5 we compare circular averages of the normalized idler counts for all cases from Fig. 4. Each point represents an average number of photon counts within a ring at radius $|\mathbf{k}^i_\perp - \mathbf{k}^i_{\perp c}|$ with unit width, where by $\mathbf{k}^i_{\perp c}$ we denote the position of the center of each phase-matching pattern from Figs. 4(f)–4(j). The actual values of $\mathbf{k}^i_{\perp c}$ are derived from Eq. (6). With this detailed view we show explicitly that correlation phase-matching patterns ranging from Gaussian-like shapes to tight rings can be engineered by controlling the spin-wave wave vector $\mathbf{K}$. Additionally, one can imagine that even more complex patterns could be obtained by preparing the initial spin wave in a superposition in k space or by reshaping the spin-wave spatial structure using, for example, ac-Stark shift [16,21,36].

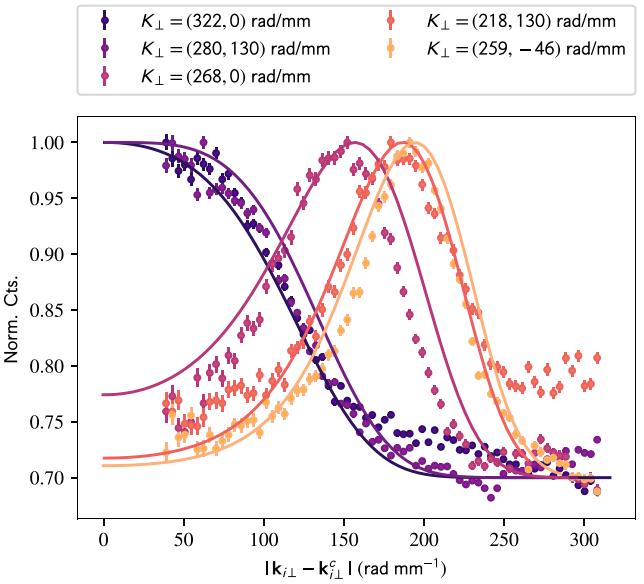

FIG. 5. Average normalized number of idler counts as a function of distance $|\mathbf{k}^i_\perp - \mathbf{k}^i_{\perp c}|$ from the center of the circular region $\mathbf{k}^c_{i\perp}$ determined by phase-matching cone. The solid lines correspond to the theoretical prediction of the phase function described by Eq. (6). Discrepancies at the edge are attributed to varying noise background.

V. CONCLUSIONS AND PERSPECTIVES

In conclusion, we have demonstrated SW-based control of superradiance in the six-wave mixing process. Our experiments pave the way towards new schemes involving specifically prepared atomic states that lead to nonstandard emission, such as, for example, subradiance [59] as well as interference in the superradiant emission. Interesting perspectives arise due to the increased range of possibilities in the wave-vector space compared with low-dimensional interfaces. With those features, applications such as optical quantum amplifiers [60] or superradiant clocks [61] can be extensively studied and optimized in atom-ensemble systems where SW control is feasible. Nowadays, extensive studies of superradiance in atomic arrays or one-dimensional interfaces [62–66], where atoms are strongly coupled to each other, distinctively reveal associated many-body quantum effects, such as cooperative resonances and cooperative Lamb shift [67,68]. Remarkably, however, even in optically dense extended free-space atomic ensembles [10] as seen in this work, superradiance plays a crucial role.

Spatial engineering of the demonstrated superradiance extends beyond fundamental aspects. In particular, control of the enhancement of the emission rate in a particular direction helps extend the bandwidth of a photon and potentially match it to a particular receiver. On the other hand, canceling the phase matching allows selective retrieval of stored atomic coherence and thus temporal multimodality.

In the more practical context, our experiment shows that photons resonant to excited–to–excited-state transitions couple to the ground-state coherence. While preliminary demonstrations for classical light have been made [31,50], here we have demonstrated quantum correlations in this scheme. This opens the path to embedding the two functions of a frequency-converted quantum repeater node [46] in a single atomic ensemble. Practically, it is beneficial to use a telecom transition (for rubidium, for example, 1529- and 1475-nm transitions leading to a $4D_{3/2}$ manifold).

Finally, it would be particularly interesting to replace one of the strong driving fields in the 6WM process by a quantum field. Essentially, generation of a single SW excitation can be heralded by detecting a photon scattered in the Raman process. Such a configuration directly leads to generation of a correlated three-photon state. Note that the process could also

be reversed—first, a single SW would be generated by heralding detection of a photon pair. The resulting state would be a three-partite entangled state of a photon pair and a collective atomic excitation. We envisage that both configurations can be achieved by increasing the two-photon excitation efficiency—currently limited by decoherence caused by the sole pump 1 field. Additionally, it would be also interesting to couple the signal field to the cavity enhancing the emission to the phase-matched region, preferably in the colinear SI configuration [Fig. 4(a)]. In this way, the brightness could even surpass the photon downconversion probability in three-photon SPDC experiments [47,69]. Such a tripartite entanglement generation scheme lends itself to two-dimensional quantum repeaters, as proposed in Ref. [70]. Our scheme would hold a direct advantage over other three-photon entanglement generation schemes in the quantum repeater context, as one of the photons is directly created as a stored spin wave, akin to the manner of the original DLCZ scheme. Furthermore, the SW could also be prepared in a deterministic way using a Rydberg blockade [22,71], and nonlinear Rydberg interactions can play an intricate role in superradiance

ACKNOWLEDGMENTS

We thank K. Banaszek for the generous support and J. H. Müller for insightful discussion. This work has been supported by the Polish Ministry of Science and Higher Education Diamentowy Grant, Projects No. DI2013 011943 and No. DI2016 014846, and the National Science Centre (Poland) through Grants No. 2016/21/B/ST2/02559, No. 2017/25/N/ST2/01163, and No. 2017/25/N/ST2/00713. The research is supported by the Foundation for Polish Science, cofinanced by the European Union under the European Regional Development Fund, as a part of the Quantum Optical Technologies project carried out within the International Research Agendas program. M.P. was supported by the Foundation for Polish Science with a START program scholarship.

APPENDIX A: EXPERIMENTAL SETUP DETAILS

We use an elongated ($\sigma_x \times \sigma_y \times \sigma_z = 0.3 \times 0.3 \times 2.5\,\mathrm{mm}^3$) ensemble of cold ($T \approx 22\ \mu\mathrm{K}$) rubidium-87 atoms in the magneto-optical trap (MOT), described in detail in Refs. [6,72]. Before the actual 6WM experiment the atoms are optically pumped to the $|g\rangle$ state [$5S_{1/2}, F = 1, m_F = 1$, see Fig. 1(a)]. To generate the macroscopic ground-state coherence $\rho_{gh}(\mathbf{r})$, where $|h\rangle = 5S_{1/2}, F = 2, m_F = -1$, we use two phase-coherent optical fields (write and seed, both 795 nm). The $\rho_{hg}(\mathbf{r})$ generation process can be understood as a stimulated (seeded with seed light) Raman scattering in the Λ system driven by the strong write light. Here, the Λ system is composed of levels $|g\rangle$, $|h\rangle$, and $|a\rangle$ ($5P_{1/2}, F = 2, m_F = 0$). In such processes, both the seed light and atomic coherence are amplified at the expense of the write field.

The seed field is derived from the write laser using a frequency-shifting setup consisting of electro-optic modulator (EOM) and a filtering Fabry-Perot cavity (see Supplemental Material of Ref. [21]). The remaining lasers (excluding pump 2) are frequency stabilized to either a cooling-and-trapping laser (780 nm) or repumping laser (795 nm) using

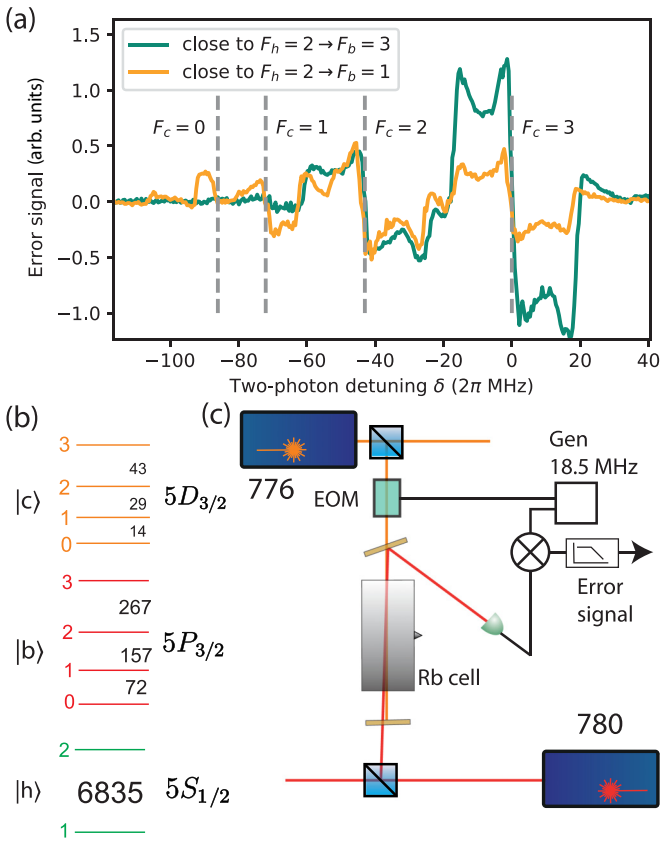

FIG. 6. Modulation transfer spectroscopy setup for locking the 776-nm laser to the two-photon resonance. The obtained error signal at two different single-photon detunings within the Doppler-broadened line is presented in (a). The two-photon detuning is measured from the resonance corresponding to $F_c = 3$. In (b) we show the relevant hyperfine energy levels with spacings between them given in MHz. Panel (c) presents the experimental setup.

the optical frequency locked loop described in [73]. The pump 2 laser at 776 nm is stabilized to the pump 1 laser using a modified version of the two-photon lock (see Fig. 6), presented in Ref. [74]. The modification employs a technique called modulation transfer spectroscopy to keep pumps 1 and 2 in two-photon resonance between levels $|g\rangle$ and $|c\rangle$. In this modulation transfer spectroscopy technique [75,76], as opposed to the simpler frequency modulation spectroscopy, we do not modulate the probe light. Instead, we modulate the coupling (776 nm) light using a phase-only EOM equipped with a custom resonant circuit and probe the system with an unmodulated beam, here at 780 nm (pump 1 laser). The modulation is thus transferred to the probe beam and is detectable in the demodulated signal if the two beams interact in the vapor cell. The probe beam is then measured and its rf (18.5 MHz) signal demodulated (mixed) with the pump modulation. Finally, the error signal is obtained after a low-pass filter. A significant advantage of this scheme is the stability of the error signal offset, as out of resonance we will simply not have any signal. Furthermore, we become nearly immune to the residual amplitude modulation of the EOM, as the amplitude modulation is transduced weakly by the atoms.

The obtained error signal as we scan the 776-nm laser is presented in Fig. 6(a). All four levels of the highest excited-state $|c\rangle$ [Fig. 6(b)] manifold are visible. By changing the single-photon detuning within the Doppler-broadened line corresponding to the $F_h = 2$ manifold, we observe relative changes of various components that arise due to selection rules.

The time domain correlation measurements were performed using Perkin-Elmer SPCMs (∼50% quantum efficiency) connected to a single-mode fibers (SMFs). The SMF are projecting the output states on Gaussian beam modes with waists of radius equal to 0.15 mm overlapping at the center of the atomic cloud. The Field-programmable gate array-based time-tagger which we use provides 3.85-ns time resolution. The spatially resolved detection is performed using homebuilt I-sCMOS camera situated in the far field of the ensemble. The far-field imaging setup was designed using ray-tracing software (ZEMAX) to maximize the field of view and resolution in k space (see [72] for more details). A detailed description of the I-sCMOS camera itself can be found in Ref. [55].

APPENDIX B: SPIN-WAVE DOWNCONVERSION

Treating the atom-light interaction induced by the weak quantum signal and idler fields as a small perturbation to the free atom density operator evolution in the presence of $\mathcal{S}$, we can obtain expressions for the coherences relevant in the signal-idler generation process: ρ_{cd} and ρ_{dg}. Next, we obtain the slowly varying amplitudes of polarization operators: $\mathcal{P}_s = nd_{dc}\rho_{cd}$, $\mathcal{P}_i = nd_{gd}\rho_{dg}$. Then, treating the excited-state spin wave as one of the interacting fields, we use the relationship: $\mathcal{P} = \epsilon_0\chi E + \epsilon_0\chi^{NL}\mathcal{S}E + \cdots$ to define the linear χ and nonlinear χ^{NL} susceptibilities. Under the assumption of a small number of excitations $|\rho_{hg}| \ll 1$ and a long lifetime of the excited state $|c\rangle$: $\Gamma_c \ll \Gamma_d$, we get

$$\chi_s = 0, \tag{B1}$$

$$\chi_i = \frac{n}{\epsilon_0\hbar}\frac{|d_{gd}|^2}{i\Gamma_d + 2\Delta}, \tag{B2}$$

$$\chi_s^{NL} = \frac{n}{\epsilon_0\hbar}\frac{d_{dc}d_{dg}}{i\Gamma_d - 2\Delta}, \tag{B3}$$

$$\chi_i^{NL} = \frac{n}{\epsilon_0\hbar}\frac{d_{gd}d_{cd}}{i\Gamma_d + 2\Delta}, \tag{B4}$$

where $\Delta = \omega_{gd} - \omega_i$. As we focus on the signal-idler generation process, only the nonlinear part is of interest. Specifically, in the interaction picture the effective Hamiltonian for this process is given by [77]

$$\mathcal{H}_{\text{eff}} = \epsilon_0 \int_V d^3\mathbf{r}\chi_i^{NL}\mathcal{S}^+E_s^-E_i^- + \text{H.c.}, \tag{B5}$$

where $\mathcal{S}^+ = \mathcal{S}e^{-i\omega_{cg}t}$, and E_j^- stands for the quantized fields operators with negative frequency [77,78] defined as follows:

$$E_j^- = \sum_{\mathbf{k}_j} E_j^* a_{\mathbf{k}_j}^\dagger e^{-i(\mathbf{k}_j\cdot\mathbf{r}-\omega_j t)}, \tag{B6}$$

where $E_j = i\sqrt{\hbar\omega_j/2\epsilon_0 n_j^2 V_q}$ with the quantization volume V_q and index of refraction n_j. The first-order perturbation theory then gives the state vector

$$\begin{aligned}|\Psi\rangle &= |0\rangle - \frac{i}{\hbar}\int dt\mathcal{H}_{\text{eff}}|0\rangle \\ &= |0\rangle + \sum_{\mathbf{k}_s}\sum_{\mathbf{k}_i} F(\mathbf{k}_s,\mathbf{k}_i)a_{\mathbf{k}_s}^\dagger a_{\mathbf{k}_i}^\dagger|0\rangle,\end{aligned} \tag{B7}$$

where F is the two-photon spectral function, which is frequently employed in descriptions of SPDC experiments [79], from which we can then obtain the approximate formulas for temporal (fixed $\{\mathbf{k}_s,\mathbf{k}_i\}$) and wave-vector-domain (time-averaged) wave functions $\psi_k(\mathbf{k}_{s\perp},\mathbf{k}_{i\perp})$ and $\psi_t(t_s,t_i)$ respectively.

[1] R. H. Dicke, Phys. Rev. **93**, 99 (1954).
[2] L.-M. M. Duan, M. D. Lukin, J. I. Cirac, P. Zoller, I. Cirac, P. Zoller, J. I. Cirac, and P. Zoller, Nature (London) **414**, 413 (2001).
[3] A. Kuzmich, W. P. Bowen, A. D. Boozer, A. Boca, C. W. Chou, L.-M. Duan, and H. J. Kimble, Nature (London) **423**, 731 (2003).
[4] C. H. van der Wal, M. D. Eisaman, A. André, R. L. Walsworth, D. F. Phillips, A. S. Zibrov, and M. D. Lukin, Science **301**, 196 (2003).
[5] L. Zhao, Y. Su, and S. Du, Phys. Rev. A **93**, 033815 (2016).
[6] M. Parniak, M. Dąbrowski, M. Mazelanik, A. Leszczyński, M. Lipka, and W. Wasilewski, Nat. Commun. **8**, 2140 (2017).
[7] Y.-F. Pu, N. Jiang, W. Chang, H.-X. Yang, C. Li, and L.-M. Duan, Nat. Commun. **8**, 15359 (2017).
[8] G. K. Gulati, B. thsan, B. Chng, A. Cerè, and C. Kurtsiefer, New J. Phys. **17**, 093034 (2015).
[9] X. Guo, Y. Mei, and S. Du, Optica **4**, 388 (2017).
[10] B. Srivathsan, G. K. Gulati, B. Chng, G. Maslennikov, D. Matsukevich, and C. Kurtsiefer, Phys. Rev. Lett. **111**, 123602 (2013).
[11] W. Zhang, D.-S. Ding, J.-S. Pan, and B.-S. Shi, Chinese Phys. Lett. **31**, 064208 (2014).
[12] K. T. Kaczmarek, P. M. Ledingham, B. Brecht, S. E. Thomas, G. S. Thekkadath, O. Lazo-Arjona, J. H. D. Munns, E. Poem, A. Feizpour, D. J. Saunders, J. Nunn, and I. A. Walmsley, Phys. Rev. A **97**, 042316 (2018).
[13] R. Finkelstein, E. Poem, O. Michel, O. Lahad, and O. Firstenberg, Sci. Adv. **4**, eaap8598 (2018).
[14] M. D. Lukin, M. Fleischhauer, R. Cote, L. M. Duan, D. Jaksch, J. I. Cirac, and P. Zoller, Phys. Rev. Lett. **87**, 037901 (2001).
[15] A. Gaëtan, Y. Miroshnychenko, T. Wilk, A. Chotia, M. Viteau, D. Comparat, P. Pillet, A. Browaeys, and P. Grangier, Nat. Phys. **5**, 115 (2009).
[16] M. Mazelanik, M. Parniak, A. Leszczyński, M. Lipka, and W. Wasilewski, npj Quantum Inf. **5**, 22 (2019).

[17] K. F. Reim, J. Nunn, X.-M. Jin, P. S. Michelberger, T. F. M. Champion, D. G. England, K. C. Lee, W. S. Kolthammer, N. K. Langford, and I. A. Walmsley, Phys. Rev. Lett. **108**, 263602 (2012).

[18] E. Saglamyurek, T. Hrushevskyi, A. Rastogi, K. Heshami, and L. J. LeBlanc, Nat. Photon. **12**, 774 (2018).

[19] G. T. Campbell, O. Pinel, M. Hosseini, T. C. Ralph, B. C. Buchler, and P. K. Lam, Phys. Rev. Lett. **113**, 063601 (2014).

[20] T. S. Yang, Z. Q. Zhou, Y. L. Hua, X. Liu, Z. F. Li, P. Y. Li, Y. Ma, C. Liu, P. J. Liang, X. Li, Y. X. Xiao, J. Hu, C. F. Li, and G. C. Guo, Nat. Commun. **9**, 3407 (2018).

[21] M. Parniak, M. Mazelanik, A. Leszczyński, M. Lipka, M. Dąbrowski, and W. Wasilewski, Phys. Rev. Lett. **122**, 063604 (2019).

[22] J. Li, M.-T. Zhou, B. Jing, X.-J. Wang, S.-J. Yang, X. Jiang, K. Mølmer, X.-H. Bao, and J.-W. Pan, Phys. Rev. Lett. **117**, 180501 (2016).

[23] P. G. Kwiat, K. Mattle, H. Weinfurter, A. Zeilinger, A. V. Sergienko, and Y. Shih, Phys. Rev. Lett. **75**, 4337 (1995).

[24] J. S. Neergaard-Nielsen, B. M. Nielsen, H. Takahashi, A. I. Vistnes, and E. S. Polzik, Opt. Express **15**, 7940 (2007).

[25] Y. Takeno, M. Yukawa, H. Yonezawa, and A. Furusawa, Opt. Express **15**, 4321 (2007).

[26] C. Qiu, S. Chen, L. Q. Chen, B. Chen, J. Guo, Z. Y. Ou, and W. Zhang, Optica **3**, 775 (2016).

[27] N. Sangouard, C. Simon, H. de Riedmatten, and N. Gisin, Rev. Mod. Phys. **83**, 33 (2011).

[28] K. Niizeki, K. Ikeda, M. Zheng, X. Xie, K. Okamura, N. Takei, N. Namekata, S. Inoue, H. Kosaka, and T. Horikiri, Appl. Phys. Express **11**, 042801 (2018).

[29] F. Wolfgramm, X. Xing, A. Cerè, A. Predojević, A. M. Steinberg, and M. W. Mitchell, Opt. Express **16**, 18145 (2008).

[30] F. Wolfgramm, Y. A. de Icaza Astiz, F. A. Beduini, A. Cerè, and M. W. Mitchell, Phys. Rev. Lett. **106**, 053602 (2011).

[31] M. Parniak, A. Leszczyński, and W. Wasilewski, Phys. Rev. A **93**, 053821 (2016).

[32] B. M. Sparkes, J. Bernu, M. Hosseini, J. Geng, Q. Glorieux, P. A. Altin, P. K. Lam, N. P. Robins, and B. C. Buchler, New J. Phys. **15**, 085027 (2013).

[33] G. Campbell, M. Hosseini, B. M. Sparkes, P. K. Lam, and B. C. Buchler, New J. Phys. **14**, 033022 (2012).

[34] D. B. Higginbottom, J. Geng, G. T. Campbell, M. Hosseini, M. T. Cao, B. M. Sparkes, J. Bernu, N. P. Robins, P. K. Lam, and B. C. Buchler, Opt. Express **23**, 24937 (2015).

[35] G. Hétet, J. J. Longdell, A. L. Alexander, P. K. Lam, and M. J. Sellars, Phys. Rev. Lett. **100**, 023601 (2008).

[36] M. Lipka, A. Leszczyński, M. Mazelanik, M. Parniak, and W. Wasilewski, Phys. Rev. Appl. **11**, 034049 (2019).

[37] B. S. Ham, Sci. Rep. **7**, 7655 (2017).

[38] B. M. Sparkes, M. Hosseini, G. Hétet, P. K. Lam, and B. C. Buchler, Phys. Rev. A **82**, 043847 (2010).

[39] Y.-S. Lee, S. M. Lee, H. Kim, and H. S. Moon, Phys. Rev. A **96**, 063832 (2017).

[40] Y.-S. Lee, S. M. Lee, H. Kim, and H. S. Moon, Opt. Express **24**, 28083 (2016).

[41] T. Jeong, Y.-S. Lee, J. Park, H. Kim, and H. S. Moon, Optica **4**, 1167 (2017).

[42] M. Parniak and W. Wasilewski, Phys. Rev. A **91**, 023418 (2015).

[43] F. E. Becerra, R. T. Willis, S. L. Rolston, and L. A. Orozco, Phys. Rev. A **78**, 013834 (2008).

[44] H. H. Jen, Phys. Rev. A **95**, 043840 (2017).

[45] T. Chanelière, D. N. Matsukevich, S. D. Jenkins, T. A. B. Kennedy, M. S. Chapman, and A. Kuzmich, Phys. Rev. Lett. **96**, 093604 (2006).

[46] A. G. Radnaev, Y. O. Dudin, R. Zhao, H. H. Jen, S. D. Jenkins, A. Kuzmich, and T. A. B. Kennedy, Nat. Phys. **6**, 894 (2010).

[47] D.-S. Ding, W. Zhang, S. Shi, Z.-Y. Zhou, Y. Li, B.-S. Shi, and G.-C. Guo, Optica **2**, 642 (2015).

[48] R. T. Willis, F. E. Becerra, L. A. Orozco, and S. L. Rolston, Opt. Express **19**, 14632 (2011).

[49] J. Park, H. Kim, and H. S. Moon, Opt. Express **25**, 32064 (2017).

[50] D.-S. Ding, Z.-Y. Zhou, B.-S. Shi, X.-B. Zou, and G.-C. Guo, arXiv:1210.3963.

[51] A. S. Kuraptsev, I. M. Sokolov, and M. D. Havey, Phys. Rev. A **96**, 023830 (2017).

[52] S. J. Roof, K. J. Kemp, M. D. Havey, and I. M. Sokolov, Phys. Rev. Lett. **117**, 073003 (2016).

[53] L. Ortiz-Gutiérrez, L. F. Muñoz-Martínez, D. F. Barros, J. E. O. Morales, R. S. N. Moreira, N. D. Alves, A. F. G. Tieco, P. L. Saldanha, and D. Felinto, Phys. Rev. Lett. **120**, 083603 (2018).

[54] B. Srivathsan, G. K. Gulati, A. Cerè, B. Chng, and C. Kurtsiefer, Phys. Rev. Lett. **113**, 163601 (2014).

[55] M. Lipka, M. Parniak, and W. Wasilewski, Appl. Phys. Lett. **112**, 211105 (2018).

[56] H. Paul, Rev. Mod. Phys. **54**, 1061 (1982).

[57] B. Zhao, Y.-A. Chen, X.-H. Bao, T. Strassel, C.-S. Chuu, X.-M. Jin, J. Schmiedmayer, Z.-S. Yuan, S. Chen, and J.-W. Pan, Nat. Phys. **5**, 95 (2009).

[58] H. H. Jen, Ann. Phys. (NY) **360**, 556 (2015).

[59] H. H. Jen, Phys. Rev. A **96**, 023814 (2017).

[60] A. A. Svidzinsky, L. Yuan, and M. O. Scully, Phys. Rev. X **3**, 041001 (2013).

[61] M. A. Norcia, M. N. Winchester, J. R. K. Cline, and J. K. Thompson, Sci. Adv. **2**, e1601231 (2016).

[62] P. Solano, P. Barberis-Blostein, F. K. Fatemi, L. A. Orozco, and S. L. Rolston, Nat. Commun. **8**, 1857 (2017).

[63] A. Asenjo-Garcia, M. Moreno-Cardoner, A. Albrecht, H. J. Kimble, and D. E. Chang, Phys. Rev. X **7**, 031024 (2017).

[64] J. D. Hood, A. Goban, A. Asenjo-Garcia, M. Lu, S.-P. Yu, D. E. Chang, and H. J. Kimble, Proc. Natl. Acad. Sci. USA **113**, 10507 (2016).

[65] A. Goban, C.-L. Hung, J. D. Hood, S.-P. Yu, J. A. Muniz, O. Painter, and H. J. Kimble, Phys. Rev. Lett. **115**, 063601 (2015).

[66] H. L. Sørensen, J.-B. Béguin, K. W. Kluge, I. Iakoupov, A. S. Sørensen, J. H. Müller, E. S. Polzik, and J. Appel, Phys. Rev. Lett. **117**, 133604 (2016).

[67] E. Shahmoon, D. S. Wild, M. D. Lukin, and S. F. Yelin, Phys.Rev. Lett. **118**, 113601 (2017).

[68] Z. Meir, O. Schwartz, E. Shahmoon, D. Oron, and R. Ozeri, Phys. Rev. Lett. **113**, 193002 (2014).

[69] H. Hübel, D. R. Hamel, A. Fedrizzi, S. Ramelow, K. J. Resch, and T. Jennewein, Nature (London) **466**, 601 (2010).

[70] J. Wallnöfer, M. Zwerger, C. Muschik, N. Sangouard, and W. Dür, Phys. Rev. A **94**, 052307 (2016).

[71] R. Wei, B. Zhao, Y. Deng, Y.-A. Chen, and J.-W. Pan, Phys. Rev. A **83**, 063623 (2011).
[72] M. Dąbrowski, M. Mazelanik, M. Parniak, A. Leszczyński, M. Lipka, and W. Wasilewski, Phys. Rev. A **98**, 042126 (2018).
[73] M. Lipka, M. Parniak, and W. Wasilewski, Appl. Phys. B **123**, 238 (2017).
[74] M. Parniak, A. Leszczyński, and W. Wasilewski, Appl. Phys. Lett. **108**, 161103 (2016).
[75] V. Negnevitsky and L. D. Turner, Opt. Express **21**, 3103 (2013).
[76] Y. N. M. de Escobar, S. P. Álvarez, S. Coop, T. Vanderbruggen, K. T. Kaczmarek, and M. W. Mitchell, Opt. Lett. **40**, 4731 (2015).
[77] J. Wen, S. Du, and M. H. Rubin, Phys. Rev. A **75**, 033809 (2007).
[78] J. Wen, S. Du, and M. H. Rubin, Phys. Rev. A **76**, 013825 (2007).
[79] M. H. Rubin, D. N. Klyshko, Y. H. Shih, and A. V. Sergienko, Phys. Rev. A **50**, 5122 (1994).